

Development of energy based Neuro-Wavelet algorithm to suppress structural vibration

Yasser Bigdeli* and Dookie Kim^a

Department of Civil Engineering, Kunsan National University, Jeonbuk, 573-701, Republic of Korea

(Received April 6, 2016, Revised February 1, 2017, Accepted February 10, 2017)

Abstract. In the present paper a new Neuro-Wavelet control algorithm is proposed based on a cost function to actively control the vibrations of structures under earthquake loads. A wavelet neural network (WNN) was developed to train the control algorithm. This algorithm is designed to control multi-degree-of-freedom (MDOF) structures which consider the geometric and material non-linearity, structural irregularity, and the incident direction of an earthquake load. The training process of the algorithm was performed by using the El-Centro 1940 earthquake record. A numerical model of a three dimensional (3D) three story building was used to accredit the control algorithm under three different seismic loads. Displacement responses and hysteretic behavior of the structure before and after the application of the controller showed that the proposed strategy can be applied effectively to suppress the structural vibrations.

Keywords: wavelet neural network; 3D building model; structural response; non-linearity; hysteretic behavior

1. Introduction

Prompted progress on material engineering contributed to identification of appropriate building materials such as high performance steel, concrete and composite materials. Applications of these materials in building construction resulted in taller, slender and flexible buildings which are sensitive to vibrations induced by earthquake and strong winds. In order to reduce such sensitivity of structures, control strategies such as active, passive, hybrid and semi active were employed to respond to this issue (Housner *et al.* 1997, Spencer and Nagarajaiah 2003, Fisco and Adeli 2011a, 2011b, Rezaee and Aly 2016). However, the performance of these methods were not perfect always. Several techniques have been used for decades to control vibration of different type of structures. Neural network (NN) techniques were used in those works as a base of the developed methods (Bigdeli and Kim 2015, 2016). Neural network was the most commonly used technique to give a solution to the non-linear complex problems where an implicit mathematical theory was not able to compute (Adeli and Hung 1994, Adeli 2001, Bigdeli *et al.* 2014). For building structures, Ghaboussi and Joghataie (1995) employed this technique to recognize the response of a 2-D multi-story building structure. Recently, this technique was being used for decades as a combination of other functions such as cost function to develop more effective algorithms (Bigdeli and Kim 2014, Kim *et al.* 2015, Bigdeli and Kim 2016a, 2016b, Kaloop *et al.* 2016). Another function used

by researchers for different purposes is the Wavelet function (Adeli and Kim 2004). The recent application of this function with control algorithm showed promising outputs that significantly reduced the structural vibration (Jiang and Adeli 2008).

Wavelet function in engineering studies was firstly used by mathematicians and seismologists who worked on seismic signal analysis (Goupillaud *et al.* 1984, Grossmann and Morlet 1984, Daubechies 1988). This function was used in various applications, for example wavelet transforms were employed for control algorithms including wavelet-hybrid feedback-Least Mean Square, fuzzy neural network and genetic algorithm, sliding mode control, analysing seismic data, and the earthquakes' prediction (Alperovich and Zheludev 1998, Edwards and Spurgeon 1998, Chu *et al.* 2002, Samali and Al-Dawod 2003, Ahmadizadeh 2007, Aly 2014).

An optimal combination of NN, wavelet functions, and a cost function is suggested in this paper to build an effective algorithm to reach the control purposes. The feasibility of this idea has been taken into investigation through modeling of regular and irregular three story buildings under various seismic loadings while the new methodology was applied to the system. In this model, the incident direction of an earthquake and time delay effects were taken into considerations. In order to make a realistic model, the actuator dynamics effects and the coupling effects between lateral and torsional responses of structure were taken into account

1.1 Wavelet function

A wavelet function includes following properties (Daubechies 1988): (1) continuity, (2) integral of this function is equal to zero (i.e., zero mean amplitude), (3)

*Corresponding author, Ph.D.
E-mail: yasse.bigdeli@gmail.com

^aProfessor
E-mail: kim2kie@gmail.com

required energy at the lower frequencies is comparatively less than that at the higher frequencies, (4) wavelets are divided into two groups of orthogonal and bi-orthogonal. A compactly supported function, the decomposition, and reconstruction processes use the same base function for orthogonal wavelet, while the bi-orthogonal wavelet is second type of the finite duration wavelet function, (5) acceptability, which certifies a full reconstruction of a primary signal of the coefficients of transformed function, (6) shape of the function is divided into two types (i.e., symmetrical and asymmetrical shapes), and (7) degree of differentiability of the wavelet function which is necessary to develop a smooth view of signals.

Orthogonal and bi-orthogonal wavelet functions are the most commonly used functions in algorithms because, some properties of these functions such as finitely supported and fast processed provide an effective and unique technique in signal analysing (Adeli and Kim 2004, Daubechies 1988).

2. Neuro-Wavelet model

2.1 Subjects included in neuro-wavelet model

Using the wavelet transform functions and wavelet coefficients, a dynamic system function can be stated as below (Daubechies 1988)

$$\bar{f}(X_{n_1}) = \sum_i w_i \sum_{a,b} \psi_{a,b}(X_{n_1}) \quad (1)$$

$$i = 1, \dots, M, a, b \in R \quad \psi \in L^2(R)$$

in which $\bar{f}(X_k)$ denotes the approximation of $f(X_{n_1})$, w_i is the discrete wavelet transform coefficient, M indicates the number of wavelets, and $\psi_{a,b}(X_{n_1})$ is a two dimensional (2-D) wavelet extension function. The basic wavelet function $\varphi(t)$ is expressed as following

$$\psi_{a,b}(X_{n_1}) = \frac{1}{\sqrt{|a|}} \varphi\left(\frac{X_{n_1} - b}{a}\right), \quad a, b \in R, \varphi \in L^2(R) \quad (2)$$

In this equation $a \neq 0$ and b represent the scale and space location vectors corresponding to the n_1 th multi-dimensional input vector X_{n_1} . R represents a set of real numbers and $L^2(R)$ states the square formed state space vector. Subscript n_1 represents the n_1 th input vector which is for simplification of the state.

A mathematical optimization approach is used to minimize the differences between approximated of the proposed Neuro-Wavelet model and actual outputs. In order to perform the error minimization process a non-orthogonal differentiable wavelet function (Mexican hat wavelet) is employed because it is a derivative wavelet function which is required to complete the process. The advantages of using Mexican hat wavelet function in comparison to the other employed functions are the unique properties of this function listed as following: (1) capability of decomposing time series signals, (2) computationally efficient, (3) amplification is non-compact nevertheless it is a sharply

vanishing function (Jiang and Adeli 2004), and (4) capability of being analytically differentiable.

The function, is stated mathematically as below

$$\varphi(t) = (D - t^2) \exp\left(-\frac{t^2}{2}\right) \quad (3)$$

Where $t = \left\| \frac{X-b}{a} \right\|$ for a multidimensional input vector

X in which $\|Y\| = \sqrt{\sum_i |y_i|^2}$ represents the Euclidean distance.

2.2 Wavelet neural network model

Fig. 1 illustrates an architectural wavelet neural network model with several layers. It consists of three layers; input layer, wavelet layer, and output layer (Hu and Kaloop 2015). The network starts with n_1 input (node) data and continues with the same number as nodes in the wavelet layer. The wavelet functions, with the same number as nodes, were applied at the wavelet layer. The weighted data from first nodes transferred to the wavelet layer (see Fig. 1). a_n and b_n are the scale and space coefficients applied to the wavelet function. These factors were modified by using a trial and error procedure. After filtering in the hidden layer, the new generated signals were sent to output layer.

A wavelet frame was also used to propagate extra specifications such as adaptable translation parameters which were desirable in the function access to make flexibility in the creation of new wavelets. Akaike's final prediction error criterion and the developed Gram-Schmidt algorithm were used to obtain a minimum number of wavelets send to select the wavelets.

The net output of hidden layer is stated as below

$$o_i^1 = f^1(net_i^1) \quad (i = 1, 2, \dots, n_2) \quad (4)$$

In which the notation n_1 represents the number of inputs. net_i^1 denotes the net input of the i th node of the hidden layer given as follows

$$net_i^1 = \sum_{h=1}^{n_1} W_{ih}^1 I_h + b_i^1 \quad (5)$$

The connection weight (W_{ih}^1) indicates the weight between the input and hidden layers. The bias of the hidden layer was b_i^1 . In the present study training is performed by minimizing a criterion expressed as

$$E = \sum |o_d - o_a|^2 \quad (6)$$

The desired output and the actual network output are respectively represented by O_d and O_a notations. By shifting the error function to zero during the training rule, actual output and developed network outputs became equal to the same value. Then, wavelet neural network finally predicts the optimal output. The proposed network can be a controller whenever the desired output used as a control signal.

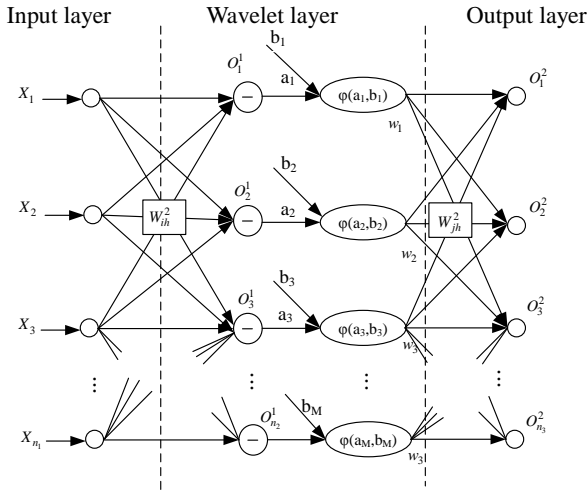


Fig. 1 Architecture of WNN model

3. Control algorithm

3.1 Control strategy and training rule

The training rule consists of combination of a cost function and a control signal. The mathematical model of training criterion is stated as following (Bigdeli and Kim 2014)

$$J = \frac{1}{2} \int_0^{T_f} (\mathbf{z}^T \mathbf{Q} \mathbf{z} + \mathbf{u}^T \mathbf{R} \mathbf{u}) dt \quad (7)$$

where

- $\mathbf{z}(n \times 1)$: state signal,
- $\mathbf{u}(m \times 1)$: control signal,
- $\mathbf{Q}(n \times n)$: weighing matrices,
- $\mathbf{R}(m \times m)$: weighing matrices,
- T_f : final time,

The first and second terms inside the integral respectively represent the vibration and control energy. The weighting matrices \mathbf{Q} and \mathbf{R} were used to non-dimensionalize the relevant terms. By application of a discrete-time domain, the cost function can be rewritten as following (Bigdeli and Kim 2014)

$$\hat{J} = \sum_{k=0}^{N_f-1} \{ \mathbf{z}_{k+1}^T \mathbf{Q} \mathbf{z}_{k+1} + \mathbf{u}_k^T \mathbf{R} \mathbf{u}_k \} = \frac{1}{2} \sum_{k=0}^{N_f-1} J_k \quad (8)$$

in which the k represents sampling number, N_f represents the total number of sampling times, and T_s denotes sampling interval. The gradient descent rule was applied to the cost function at the k -th step. Thus, at this step the weight update, W_{ji}^2 is

$$\Delta W_{ji}^2 = -\eta \frac{\partial \hat{J}_k}{\partial W_{ji}^2} \quad (8)$$

In which η indicates the training rate. The convergence of training corresponding to the training rate change can be modified. The partial derivative of Eq. (9) is expressed as following

$$\frac{\partial \hat{J}_k}{\partial W_{ji}^2} = \frac{\partial \hat{J}_k}{\partial net_j^2} \frac{\partial net_j^2}{\partial W_{ji}^2} \quad (10)$$

Then, the generalized error can be expressed as following

$$\delta_j^2 = -\frac{\partial \hat{J}_k}{\partial net_j^2} = -\frac{\partial \hat{J}_k}{\partial o_j^2} \frac{\partial o_j^2}{\partial net_j^2} \quad (11)$$

weight update is

$$\Delta W_{ji}^2 = \eta \delta_j^2 o_i^1 \quad (12)$$

in which

$$\delta_j^2 = -\left(\mathbf{z}_{k+1}^T \mathbf{Q} \left\{ \frac{\partial \mathbf{z}_{k+1}}{\partial \mathbf{u}_{k,j}} \right\} + \mathbf{u}_k^T \mathbf{r}_j \right) \mathbf{G}_j(f^2) \Big|_{net_j^2} \quad (13)$$

where, all the terms are available at the k th step, and \mathbf{G}_j covers

$$\mathbf{u}_j = \mathbf{G}_j \mathbf{o}_j^1 \quad (14)$$

Where \mathbf{r}_j is the j th column vector of \mathbf{R} .

The bias update is

$$\Delta b_j^2 = \eta \delta_j^2 \quad (14)$$

update for the weight, W_{ji}^1 , is determined in the same way, as

$$W_{ji}^1 = \eta \delta_j^1 I_h \quad (16)$$

in which

$$\delta_j^1 = -\frac{\partial \hat{J}_k}{\partial net_j^1} = -\sum_{j=1}^{n_3} \frac{\partial \hat{J}_k}{\partial net_j^2} \frac{\partial net_j^2}{\partial o_i^1} \frac{\partial o_j^1}{\partial net_j^1} = \sum_{j=1}^{n_3} \delta_j^2 W_{ji}^2 (f^1) \Big|_{net_j^1} \quad (17)$$

and the bias update of the hidden layer is

$$\Delta b_i^1 = \eta \delta_i^1 \quad (18)$$

3.2 Non-linear dynamic model of irregular 3d building model

Almost all of building structures have kind of irregularity in their plan or elevation. It especially is due to the different properties of material in use to construct the building elements. As a result, different story stiffness along the two principal directions is another proof of that. Such differences could lead to distance between the center of mass (CM) and center of resistant (CR) in each floor. Thus, CR and CM do not lie on a vertical straight line through the elevation of an actual building that can affect the behavior of the structure. In such condition a lateral-

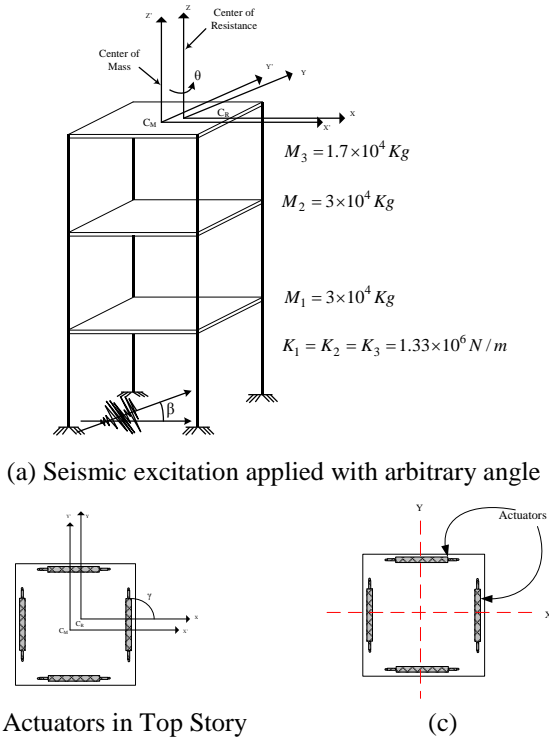


Fig. 2 Structural model (a) 3D building and (b), and (c) typical story with four actuators

torsional coupling behavior can occur, which usually underestimate the maximum response of a structure subjected to dynamic loads (Jiang and Adeli 2004).

In this research selected building model has following properties: (1) floors are rigid, and (2) columns of the building have no axial deformations along the vertical axis. The degree of freedom (DOFs) at each floor consists of three components including translations in two main directions and a rotation about vertical z axis passing across the CM points identified on each floor. Thus, for an m -story building the summation of DOFs for whole building was $n=3m$. The vector of structural displacement response at the time t was obtained as following

$$\begin{aligned} u(t) &= [u_1(t) \ u_2(t) \dots \ u_m(t) \ v_1(t) \dots \\ v_2(t) \ v_m(t) \ \theta_1(t) \ \theta_2(t) \dots \ \theta_m(t)]_{3m \times 1}^T \end{aligned} \quad (19)$$

in which the notations are as following: $u_i(t)$: translation in x directions, $v_i(t)$: translation in the y directions, $\theta_i(t)$: rotation around the vertical axis z of the i -th floor, and T : transpose of a matrix. The dominant equation of motion for a structural coupled system consists a 3-D building structure and an active control system. When the system was subjected to an excitation signal, the equation of motion was expressed as following

$$\mathbf{M}\ddot{\mathbf{u}}(t) + \mathbf{C}\dot{\mathbf{u}}(t) + \mathbf{R}(x, t) = \mathbf{I}_c F(t) - \mathbf{M}_0 \mathbf{I}_g \ddot{\mathbf{x}}(t) \quad (20)$$

In which the notations represent the following parameters: \mathbf{M} : an $(n \times n)$ mass matrix; \mathbf{C} : an $(n \times n)$ damping matrix; $\mathbf{R}(x, t)$: an $(n \times 1)$ restoring force signal; \mathbf{I}_c : an $(n \times n)$ location matrix which is related to the actuators location; $F(t)$: an $(n \times 1)$ signal of control force in which the elements

are in time series format; $\ddot{\mathbf{x}}_g$: an earthquake acceleration signal applied in an arbitrary and horizontal direction, and \mathbf{M}_0 : an $(n \times n)$ diagonal mass matrix. The arrays of diagonal mass matrix are the same as the diagonal arrays of the full mass matrix (\mathbf{M}).

In the present study, two pairs of actuators are employed in an Active Mass Damper (AMD) system at the roof along with two perpendicular axes, x and y (see Fig. 3(b)). Actuators were designed to apply the control force $F(t)$ in the corresponding directions. The control force is assigned to the couple of actuators in a way to prevent from causing of any moment by actuators. The eccentricity (i.e., distance between the CM and CR) which may happen due to non-uniformity of material or geometry in each floor were neglected to simplify the computation. Therefore, the activation of actuators not only will not cause moment by themselves but also will not contribute to the rotation response of structure due to eccentricity. The orientations of actuators installed at the roof were at $\delta=0^\circ$ and $\delta=90^\circ$ for two couples of actuators (see Fig. 2).

In Eq. (20), \mathbf{I}_g is an $n \times 1$ orientation matrix representing the direction of an applied earthquake load. The orientation matrix was stated as following

$$\begin{aligned} \mathbf{I}_g &= [\cos(\beta) \ \cos(\beta) \ \cos(\beta) \ \cos(\beta) \dots, \\ &\sin(\beta) \ \sin(\beta) \ \sin(\beta) \ \sin(\beta) \dots, \ 0 \ 0 \ 0 \ 0 \dots]_{n \times 1} \end{aligned} \quad (21)$$

in which, the direction angle of a seismic load was measured from x -axis, is denoted by β (see Fig. 2(a)). The applied earthquake excitation signal was in a time-series form and belonged with the horizontal components of ground motion record. As the earthquake excitation applies to the structural model, the recorded response of the top floor, $u(t)$, in both x - and y -directions and earthquake signal itself transferred to the controller. The control force generated by the AMD system was used to mitigate the displacement response of the structure at the top floor of the building for every step. According to the properties of the actuators, control forces were generated corresponding to an electric control signal. Following this process, the actuators were motivated by the control signal to generate the required control force.

3.3 Training the controller

The proposed neuro-wavelet controller model uses three layers of networks however the number of layers corresponding to amount of computation could be increased. First layer called input layer includes nine nodes to receive the feedback of three displacements (i.e., displacement in x and y directions, and rotation θ), the velocity of top floor, and an earthquake excitation. Middle layers are called wavelet layers consisted of nine nodes for each layer receiving the outputs of the first layer. Depending on the complexity of the problem different numbers of layers may be needed. Third layer is called output layer and consists of three nodes which generates control signal in all three directions (i.e., x , y -directions and rotation θ). The state of third floor was apply to a cost function at each step. In order to develop a train criterion, the cost function was formulated at k -th step as follows

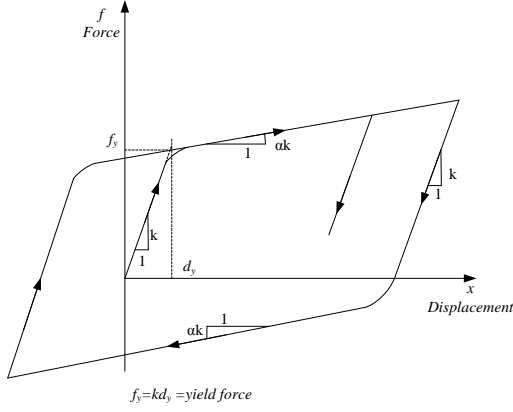


Fig. 3 Load-displacement curve for an element considering material non-linearity and hysteretic behavior

$$\hat{J}_k = \mathbf{z}_{3,k+1}^T \mathbf{Q} \mathbf{z}_{3,k+1} + r u_k^2 \quad (22)$$

in which $\mathbf{z}_{3,k+1}^T$ and u_k indicate the state of the top floor of the structure and the control signal respectively. \mathbf{Q} and r denote weighting matrices which are expressed as follows

$$\mathbf{Q} = \begin{pmatrix} \left| \frac{1}{\tilde{x}_3} \right|^2 & 0 \\ 0 & \left| \frac{1}{\tilde{\dot{x}}_3} \right|^2 \end{pmatrix} \quad (23)$$

$$r = 0.1 \left| \frac{1}{\tilde{u}} \right|^2 \quad (24)$$

where the notations are representing following parameters: \tilde{u} : maximum input control voltage, \tilde{x}_3 : maximum displacement of top floor, and $\tilde{\dot{x}}_3$: maximum velocity of top floor. In this equation, \tilde{x}_3 and $\tilde{\dot{x}}_3$ are obtained under El-Centro earthquake while the control input was off. Peak ground acceleration (PGA) of earthquake record used for training, was 0.348g where g represents the gravitational acceleration. The history of cost function for non-linear cases was recorded during the process and is shown in Fig. 4.

3.4 Hydraulic actuator

In this study the interaction between the installed actuators and structure was taken into account because, it could result in a different response of the structure armed with an AMD. Sets of linear hydraulic type of identical actuators were employed to generate an appropriate control force. This actuators provided large amount of force with as small response delay-time as milli-second, however, the required power to run the system and produce enough control force was also very small. Additionally, a hydraulic actuator can produce about 1,000 kN of force which is enough to control the response of a residential building structure. The actuators were acting simultaneously in both

Table 1 Properties provided for an actuator

Variables	Description	value
a_r	Area of piston	$3.368 \times 10^{-3} \text{ m}^2$
v	Volume of the cylinder	$1.01 \times 10^{-3} \text{ m}^3$
c_l	Leakage coefficient	$0.1 \times 10^{-10} \text{ m}^5/(\text{Ns})$
c_c	Compressibility coefficient	$2.1 \times 10^{10} \text{ N/m}$
q_{\max}	Maximum flow rate of oil	$2.0 \times 10^{-3} \text{ m}^3/\text{s}$
τ	valve time constant	0.15 Sec
g	valve constant	$2.1 \times 10^{-4} \text{ m}^3/\text{volt}$

main horizontal x and y directions to avoid causing moment (see Fig. 2(c)).

The equation of motion was derived for a hydraulic actuator that is expressed as following equations (De Silva 1989, Dyke *et al.* 1995)

$$\frac{\tau}{g} \dot{q} + \frac{1}{g} q = u \quad (25)$$

$$a_r \dot{x}_r + \frac{c_l}{a_r} f + \frac{v}{2c_c a_r} \dot{f} = q \quad (26)$$

Eq. (25) presents the valve dynamics and the Eq. (26) presents the piston's behavior. Following notations denote: g: valve constant; τ : time constant of the valve; q: flow rate of oil; and u: control signal. In the Eq. (26) a_r , c_c , c_l , and V respectively represent the area of piston, compressibility coefficient, leakage coefficient, and the volume of its cylinder, x_r is the relative displacement between the roof and piston, and f denotes the force applied on the structure by AMD system.

4. Results and discussions

4.1 non-linear dynamic model

Baber and Wen (1981) proposed a nonlinear dynamic model capable of simulating the nonlinear behavior of a structural system. This model is used in the several studies (Bani-Hani and Ghaboussi 1998). Based on this theory the restoring force consists of two linear and non-linear parts expressed as follows

$$k_s(x_s, \dot{x}_s) = \alpha k_0 x_s + (1-\alpha) k_0 d_y y \quad (27)$$

In which, $\alpha k_0 x_s$ is a linear term and $(1-\alpha) k_0 d_y y$ indicates a non-linear term of the restoring force, and x_s represents the displacement of element. As it is shown in the load-displacement curve (Fig. 3), k_0 and αk_0 ($\alpha < 1$) respectively are the slope factors of the elastic and inelastic behaviors.

By mathematically solving the following non-linear differential equation, the hysteretic variable y is determined by using following relationship

$$\dot{y} = \frac{1}{d_y} (\rho \dot{x}_s - \mu |\dot{x}_s| |y|^{p-1} - \sigma \dot{x}_s |y|^p) \quad (28)$$

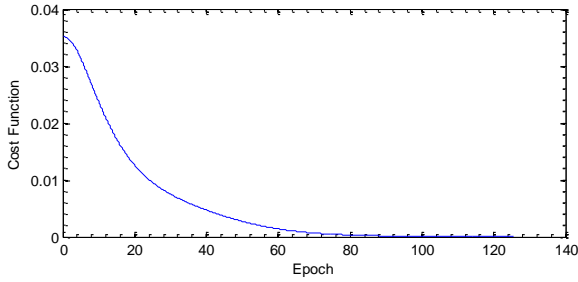


Fig. 4 Learning history

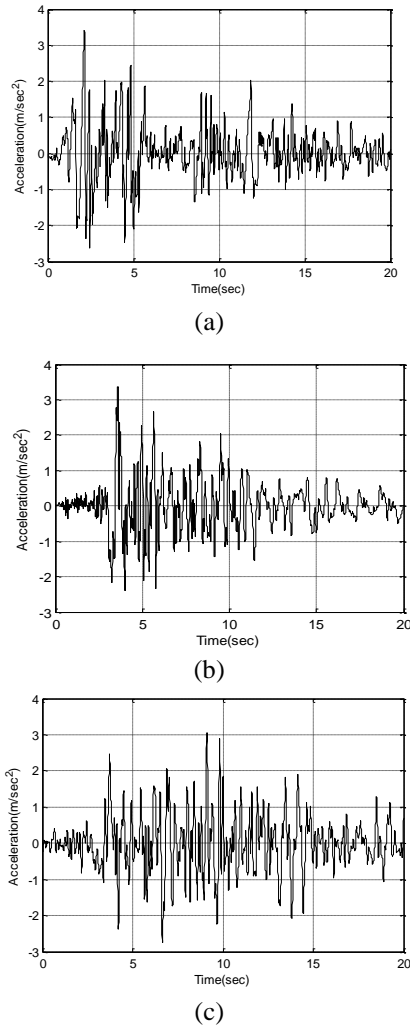
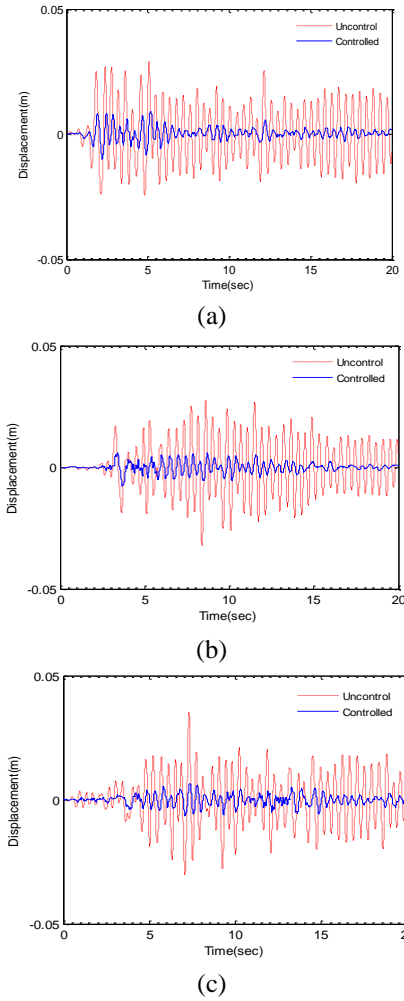


Fig. 5 Employed earthquake signals to study the behavior of the building (a) El-Centro earthquake, (b) Northridge earthquake, and (c) California earthquake

In which, ρ , μ and σ define the hysteretic behavior of the system. It worth to note that the limitation range of hysteretic variable was $-1 \leq y \leq 1$.

4.2 Example of building model

The properties of the structural model were expressed as follows: using ACI (2008) standard's provisions, the computed mass for the first, second and third stories were equal to 3×10^4 , 3×10^4 and 1.7×10^4 kg respectively. For the

Fig. 6 Uncontrolled and controlled displacement response of third floor of structure under (a) El-Centro earthquake acceleration, (b) Northridge earthquake acceleration, (c) California earthquake acceleration for $\beta=45^\circ$

first, second and third floor, the moments of inertia for diaphragms were equal to 8×10^4 , 8×10^4 , 4.533×10^4 kg.m², respectively. The inter-story stiffness in two x - and y -directions was equal to 1.33×10^6 N/m (Fig. 2). The irregularity of structure were taken into account by application of specific distance between center of masses and center of rigidities. The required damping matrix was determined by using Rayleigh damping equation represented as following (Chopra 1995)

$$\mathbf{C} = a_1 \mathbf{M} + a_2 \mathbf{K} \quad (29)$$

where a_1 and a_2 are coefficients with units of sec^{-1} and sec , respectively.

The sampling time is 0.005s and the delay time is considered as 0.0005s. The equation of motion is integrated at every 0.00025s; using Matlab coding program (Matlab 2013). The actuator properties are based on data provided by a producer (<http://www.mts.com>) which are listed in Table 1.

The computing process of the control signal and its application to the actuators took very small amount of time

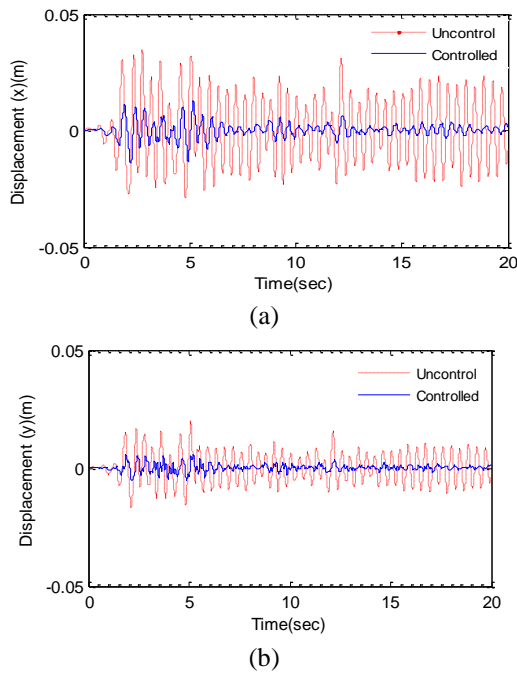


Fig. 7 Uncontrolled (red color line) and controlled (blue color line) response comparison of the third floor of a three story building under El-Centro earthquake with $\beta=30^\circ$, (a) response in x -direction (b) response in y -direction

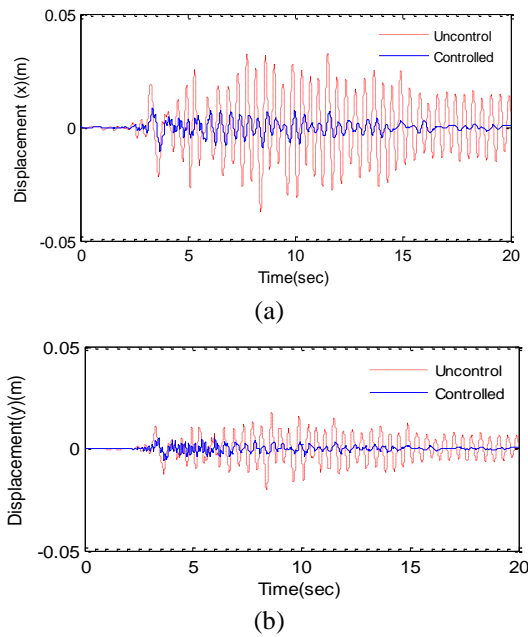


Fig. 8 Uncontrolled (red color line) and controlled (blue color line) response comparison of the third floor of a three story building under Northridge earthquake with $\beta=30^\circ$, (a) response in x -direction (b) response in y -direction

that resulted in a delay time in the process. The application of time delay to the controller is very important because it may affect the accuracy of the results. For this reason, it was taken into consideration. The control signal was determined by using a feedback signal, which was obtained by identification of z_k through the k -th sampling time step.

Table 2 Maximum displacements of top floor of 3-story structure subjected to three earthquake ground accelerations

Earthquake	Direction	Uncontrolled (m)	Controlled (m)	Reduction (%)
Northridge	x	0.0375	0.0101	73.06
	y	0.0375	0.0101	73.06
Northridge	x	0.0433	0.014	67.60
	y	0.02108	0.00709	66.36
El-Centro	x	0.0351	0.0076	78.34
	y	0.0351	0.0076	78.34
El-Centro	x	0.0412	0.00715	82.60
	y	0.0240	0.0068	71.60
California	x	0.039	0.0105	73.07
	y	0.039	0.0105	73.07
California	x	0.0441	0.0141	68.00
	y	0.0236	0.0082	65.25

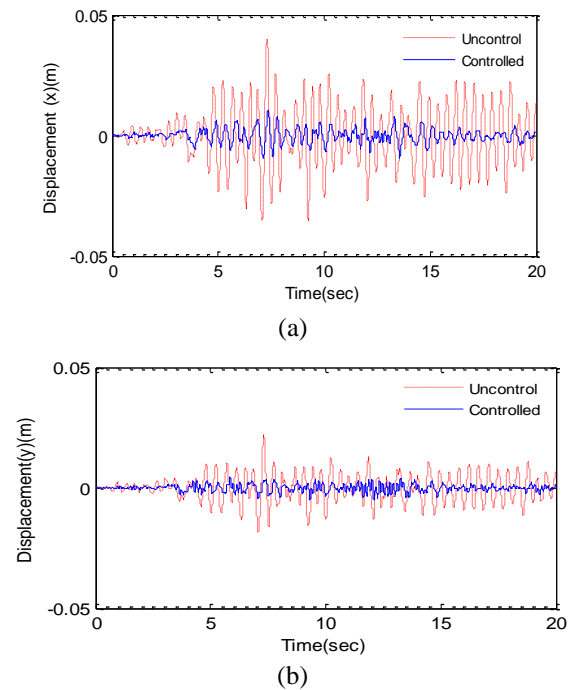


Fig. 9 Uncontrolled (red color line) and controlled (blue color line) response comparison of the third floor of a three story building under California earthquake with $\beta=30^\circ$, (a) response in x -direction (b) response in y -direction

The computation of the control signal was time consuming. Therefore, the control signal was applied at the time kT_s plus the delayed time rather than kT_s . The performance of the controller could be unsatisfied if the time delay was ignored from the process.

In order to study the behavior of the building for different loadings, various earthquake loads including El-Centro (see Fig. 4(a)), Northridge (see Fig. 4 (b)), and California (see Fig. 4 (c)) were applied to the system with arbitrary directions. Additionally, the horizontal component of El-Centro earthquake record was applied to the system with a direction angle of $\beta=45^\circ$ to perform training process of the control algorithm.

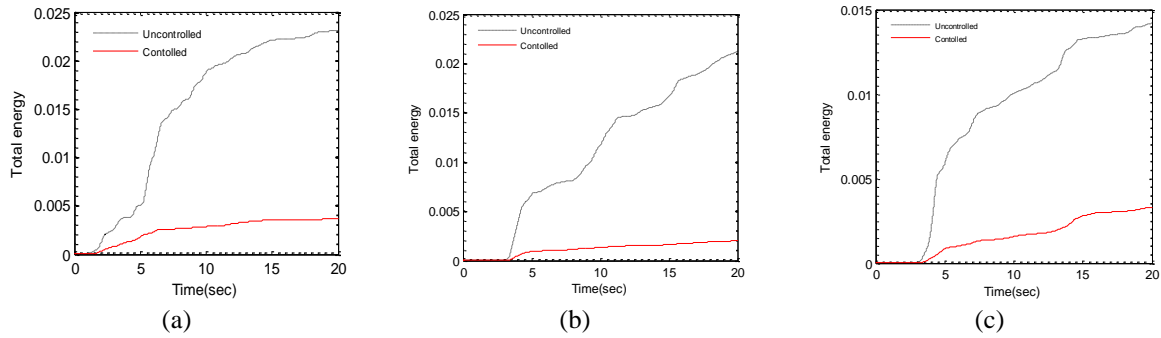
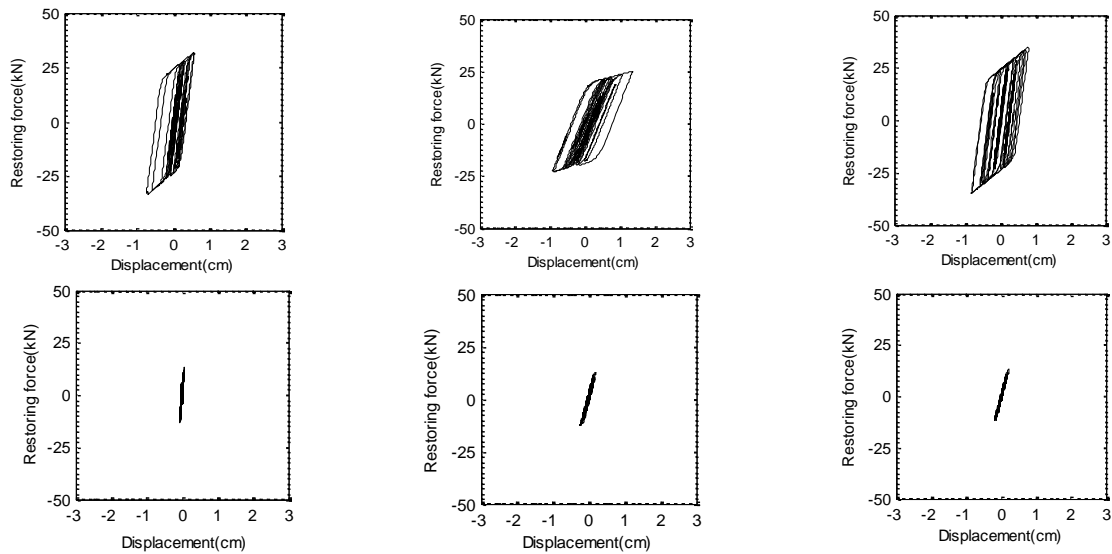


Fig. 10 Modal energy of the controlled and uncontrolled structure under (a) El-Centro earthquake, (b) Northridge earthquake, (c) California earthquake, when $\beta=45^\circ$



Third floor- El-Centro earthquake Third floor- Northridge earthquake Third floor- California earthquake

Fig. 11 Restoring force versus displacement when $\beta=45^\circ$ (up row uncontrolled; down row controlled)

4.3 Control results

The excitation signals applied to the system in arbitrary directions (β) where the simulation results of controlled and un-controlled buildings shows that the irregular structure indicates a significant vibration. It is noted that the interactions of coupled lateral and torsional behaviors were also considered in the computing process. By analyzing the simulation results, it was observed that the response of structure in terms of velocity, acceleration, and displacement, were decreased significantly (see Fig. 6). Additionally, the total modal energy was declined considerably in all cases as the controlled system was applied (see Fig. 10). Controlled displacement responses of the building were captured for three loadings and the results. The uncontrolled system subjected to the similar loadings were used as a reference for comparison. The controlled system showed a significantly smaller values for displacements for all types of loadings with any directions. In order to illustrate the results in a better visualizations, the graphical response of the structure subjected to earthquakes with angle of directions $\beta=45^\circ$ and $\beta=30^\circ$ were presented.

For $\beta=45^\circ$, the results are illustrated for the controlled

and uncontrolled building subjected to El-Centro earthquake acceleration (see Fig. 6(a)), Northridge earthquake acceleration (see Fig. 6(b)), and California earthquake (see Fig. 6(c)). For all cases a significant reductions in the responses were obtained (see Table 2). For $\beta=30^\circ$, the structural responses are illustrated in both x and y directions for the structure subjected to El-Centro earthquake acceleration (see Fig. 7), Northridge earthquake acceleration (see Fig. 8(a) and (b)). California earthquake (see Fig. 9). Table 2 reports the reduction percentages for all cases, in which the values are the same for x and y directions for $\beta=45^\circ$ because the structure was modeled as a symmetrical building and these results were expected. Furthermore, modal energy of the controlled and uncontrolled building subjected to the El-Centro earthquake (see Fig. 10(a)), Northridge earthquake (see Fig. 10 (b)), and California earthquake (see Fig. 10 (c)) was also considerably decreased. The restoring force also was taken into comparison which is shown in Fig. 11. This parameter was also drastically declined for the structure controlled using the proposed algorithm.

The maximum reductions in vibration mitigation were 73.06, 78.34 and 73.07 percent for the controlled structures

subjected to Northridge, El-Centro and California earthquake excitations, respectively (see Table 2). The vibration reduction values obtained by application of proposed algorithm looks promising in comparison to the control algorithms developed in other studies (Jiang and Adeli 2008, Jiang and Adeli 2008). The advances of the proposed neuro-wavelet algorithm can be listed as following: (1) combination of neural network, wavelet and cost function in a one algorithm, (2) reduction in the training time, and (3) application of the proposed control strategy mitigated the structural vibration very effectively.

5. Conclusions

In this paper, a wavelet neural network methodology is proposed as an algorithm with capability to reduce the vibrations of irregular three-dimensional buildings. The proposed algorithm was applied to a regular 3-D three story building to evaluate its efficiency. The geometric and material non-linearity, structural irregularity, and the incident direction of earthquake were taken into consideration in the control statement. The lateral-torsional coupling and the actuator dynamics were also considered in the control model.

The advantage of using this algorithm and methodology is the installation of actuators only at the top floor of the building while the similar strategies need to install at least two pairs of actuators in each floor of the structure which is beneficiary from economic point of view. The merits of this work can be summarized in three main properties: (1) a significant reduction of both structural response and modal energy subjected to incident direction of earthquake, (2) reduction of unfavorable interaction effects among the nodes of the wavelet neural network, and (3) the neural network training process operates faster, and calculation efficiency is improved.

Acknowledgments

This work was supported by the National Research Foundation of Korea Grant funded by the Korean Government (NRF-2014R1A2A1A10049538)

References

- ACI, Building code requirements for structural concrete (ACI 318-08) and commentary, American Concrete Institute.
- Adeli, H. (2001), "Neural networks in civil engineering: 1989-2000", *Comput. Aid. Civi Infrastr. Eng.*, **16**(2), 126-142.
- Adeli, H. and Hung, S.L. (1994), *Machine Learning: Neural Networks, Genetic Algorithms, and Fuzzy Systems*, John Wiley & Sons, Inc.
- Adeli, H. and Kim, H. (2004), "Wavelet-hybrid feedback-least mean square algorithm for robust control of structures", *J. Struct. Eng.*, **130**(1), 128-137.
- Ahmadizadeh, M. (2007), "On equivalent passive structural control systems for semi-active control using viscous fluid dampers", *Struct. Control Hlth. Monit.*, **14**(6), 858-875.
- Alperovich, L. and Zheludev, V. (1998), "Wavelet transform as a tool for detection of geomagnetic precursors of earthquakes", *Phys. Chem. Earth*, **23**(9), 965-967.
- Aly, A.M. (2014), "Proposed robust tuned mass damper for response mitigation in buildings exposed to multidirectional wind", *Struct. Des. Tall Spec. Build.*, **23**(9) 664-691.
- Bigdeli, Y. and Kim, D. (2014), "Active control of 3-D irregular building by using energy based neuro-controller", *Adv. Struct. Eng.*, **17**(6), 837-850.
- Bigdeli, Y. and Kim, D. (2015), "Response control of irregular structures using structure-TLCD coupled system under seismic excitations", *KSCE J. Civil Eng.*, **19**(3), 672-681.
- Bigdeli, Y. and Kim, D. (2016a), "Damping effects of the passive control devices on structural vibration control: TMD, TLC and TLCD for varying total masses", *KSCE J. Civil Eng.*, **20**(1), 301-308.
- Bigdeli, Y. and Kim, D. (2016b), "Investigation of the performance of two passive controllers in mitigating the rotational response of irregular buildings", *Adv. Mater. Sci. Eng.*, **2016**, Article ID 1898792.
- Bigdeli, Y., Kim, D. and Chang, S. (2014), "Vibration control of 3D irregular buildings by using developed neuro-controller strategy", *Struct. Eng. Mech.*, **49**(6), 687-703.
- Chopra, A.K. (1995), *Dynamics of Structures*, New Jersey: Prentice Hall.
- Chu, S., Soong, T., Reinhorn, A., Helgeson, R. and Riley, M. (2002), "Integration issues in implementation of structural control systems", *J. Struct. Control*, **9**(1), 31-58.
- Daubechies, I. (1988), "Orthonormal bases of compactly supported wavelets", *Commun. Pure Appl. Math.*, **41**(7), 909-996.
- De Silva, C.W. (1989), *Control Sensors and Actuators*, Prentice Hall Englewood Cliffs, NJ.
- Dyke, S., Spencer Jr, B., Quast, P. and Sain, M. (1995), "Role of control-structure interaction in protective system design", *J. Eng. Mech.*, **121**(2), 322-338.
- Edwards, C. and Spurgeon, S. (1998), *Sliding Mode Control: Theory and Applications*, CRC Press.
- Fisco, N. and Adeli, H. (2011a), "Smart structures: part I-active and semi-active control", *Scientia Iranica*, **18**(3), 275-284.
- Fisco, N. and Adeli, H. (2011b), "Smart structures: part II-hybrid control systems and control strategies", *Scientia Iranica*, **18**(3), 285-295.
- Ghaboussi, J. and Joghataie, A. (1995), "Active control of structures using neural networks", *J. Eng. Mech.*, **121**(4), 555-567.
- Goupillaud, P., Grossmann, A. and Morlet, J. (1984), "Cycle-octave and related transforms in seismic signal analysis", *Geoexplor.*, **23**(1), 85-102.
- Grossmann, A. and Morlet, J. (1984), "Decomposition of Hardy functions into square integrable wavelets of constant shape", *SIAM J. Math. Anal.*, **15**(4), 723-736.
- Housner, G., Bergman, L.A., Caughey, T.K., Chassiakos, A.G., Claus, R.O., Masri, S.F., Skelton, R.E., Soong, T.T., Spencer, B.F. and Yao, J.T., (1997), "Structural control: past, present, and future", *J. Eng. Mech.*, **123**(9), 897-971.
- Hu, J.W. and Kaloop, M.R. (2015), "Single input-single output identification thermal response model of bridge using nonlinear ARX with wavelet networks", *J. Mech. Sci. Technol.*, **29**(7), 2817-2826.
- Jiang, X. and Adeli, H. (2004), "Wavelet packet-autocorrelation function method for traffic flow pattern analysis", *Comput. Aid. Civil Infrastr. Eng.*, **19**(5), 324-337.
- Jiang, X. and Adeli, H. (2008), "Dynamic fuzzy wavelet neuroemulator for non-linear control of irregular building structures", *Int. J. Numer. Meth. Eng.*, **74**(7), 1045-1066.
- Kaloop, M.R., Hu, J.W. and Bigdeli, Y. (2016), "Identification of the response of a controlled building structure subjected to

- seismic load by using nonlinear system models”, *Appl. Scie.*, **6**(10), 301.
- Kim, D., Hassan, M.K., Chang, S. and Bigdeli, Y. (2015), “Nonlinear vibration control of 3D irregular structures subjected to seismic loads”, *Handbook of Research on Advanced Computational Techniques for Simulation-Based Engineering*, **103**.
- Matlab (2013), The MathWorks Inc., Version 2013a.
- Rezaee, M. and Aly, A.M. (2016), “Vibration control in wind turbines for performance enhancement: A comparative study”, *Wind Struct.*, **22**(1), 107-131.
- Samali, B. and Al-Dawod, M. (2003), “Performance of a five-storey benchmark model using an active tuned mass damper and a fuzzy controller”, *Eng. Struct.*, **25**(13), 1597-1610.
- Spencer Jr, B.F. and Nagarajaiah, S. (2003), “State of the art of structural control”, *J. Struct. Eng.*, **129**(7), 845-856.